Electronic Supplementary Material (ESI) for Physical Chemistry Chemical Physics.

Supplementary Information

The importance of the bacterial cell wall in Uranium (VI) biosorption

Joseph Hufton *[a], John Harding [b], Thomas J. Smith [c] and Maria Romero-González*[ad]

[a.] Department of Geography, The University of Sheffield, Sheffield, S10 2TN, UK.
Email: j.m.hufton@sheffield.ac.uk, m.romero-gonzalez@qmul.ac.uk
[b.] Department of Materials Science and Engineering, Sir Robert Hadfield Building, University of Sheffield, Mappin Street, Sheffield, S1 3JD, UK.
[c.] Biomolecular Sciences Centre, Sheffield Hallam University, City Campus, Sheffield S1 1WB, UK
[d.] School of Engineering and Materials Science (SEMS), Queen Mary University of London,12Mile End Road, London E1 4NS

Supplementary Information 1: Detailed interpretation of high resolution XPS spectra of cell surface isolates.

The high-resolution N1s spectra (Supplementary Figure 1J-L) and Supplementary Figure 2J-L) for both strains and their cell surface isolates showed peaks at ~ 400.0eV and at ~ 401.7 eV, corresponding to non-protonated and protonated nitrogenous groups respectively, and were ascribed to amides and amines in proteins [1-5]. The high percentage of non-protonated nitrogenous groups contributed to the overall net-negative charge of the cell surface isolates. The high-resolution P2p spectra (Supplementary Figure 1M-O and Supplementary Figure 2M-O) at ~ 133.7 eV corresponded to phosphodiester bonds in phosphate groups found in phospholipids and phosphorylated biomolecules [2, 4]. A high-resolution scan of the C1s regions (Supplementary Figure 1D-F and Supplementary Figure 2D-F) showed 4 components; carbon-carbon and carbon-hydrogen interactions at 285 eV, carbon bound to oxygen or nitrogen at ~ 286.47 eV (most likely from amides in proteins), a carbon-oxygen double bonded group corresponding to carbonyl, carboxylate or amide at 288.01 eV and carboxyl groups at 289 eV [1-4]. An additional peak, at about 293 eV in some samples, corresponds to carbon satellite peaks and is not taken into consideration for analysis. These satellite peaks cannot be ascribed to carbon-associated functional groups since their appearance was due to strong electron shake up excitations of the final chemical state resulting in additional peaks several eV higher than the main C1s peak at 285 eV [6]. The high resolution scan O1s peak was fitted to 2 components at 531.4 eV corresponding to carbon - oxygen and phosphorus - oxygen double bonds from carboxyl, amides and phosphate groups while the peak at 532.8 eV corresponded to oxygen present within hydroxyl and phosphate groups.

The functional groups identified above confirm the presence of polysaccharide-like material, proteins and hydrocarbon chains in the outermost layer of each sample analysed. Changes in the percentage area of certain peaks were attributed to the relative abundance of the functional groups present within each fraction. For example, there was an increase in percentage area of the O1s peak at 531.4 eV with respect to the peak at 532.8 eV between the *P. putida* intact cells (39.6 %), their cell wall (48.8 %) and membrane (59.5 %) isolates (Supplementary Figure 1G-I). This suggested an increase in the number of carboxyl, phosphate groups and amides like those present within the phospholipid bilayer and proteins present within the cell wall and membrane of Gram-negative bacteria [1-4, 7]. This was also evident in changes of the relative percentage area of the O1s peaks of *B. subtilis* intact cells (40.3 %) and their cell wall and membrane isolates (Supplementary Figure 2G-I). There was an increase in the relative percentage area of the peak at 531.4 eV in membrane isolates (61.3 %) while there was a decrease in percentage area in cell wall isolates (30.6 %). This decrease was attributed to the increase in the number of carbonyl groups present within the carbohydrate rich cell wall region which contains a majority of peptidoglycan and teichoic acids, whereas within intact cells the penetration depth of the X-ray could take into account elements present within the cell membrane as well, for example if the intact cells were ruptured.

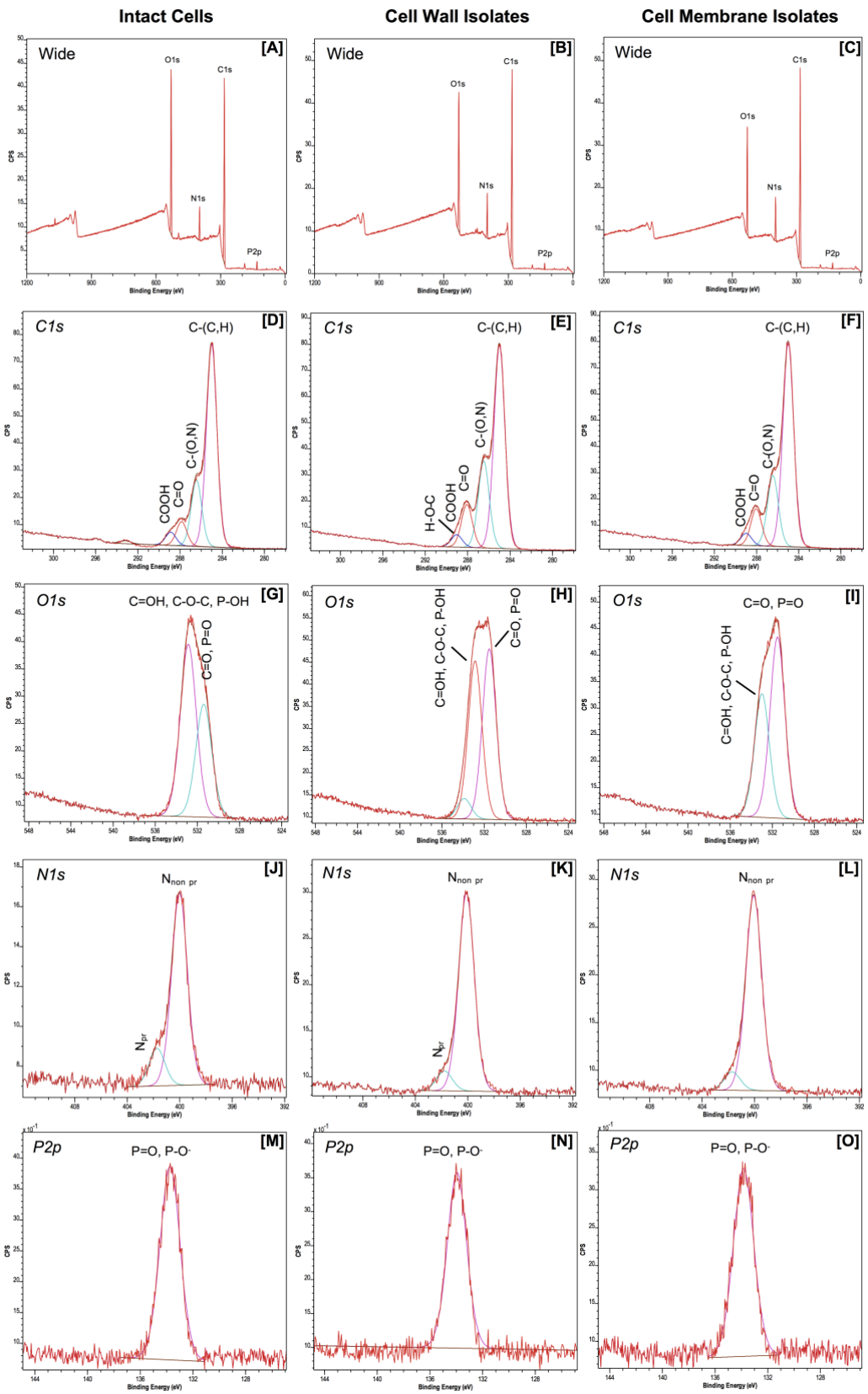

Supplementary Figure 1: XPS wide and high resolution C1s, O1s, N1s and P2p scans of intact *P. putida* 33015 cells [A, D, G, J, M], cell wall isolates [B, E, H, K, N] and cell membrane isolates [C, F, I, L, O], respectively.

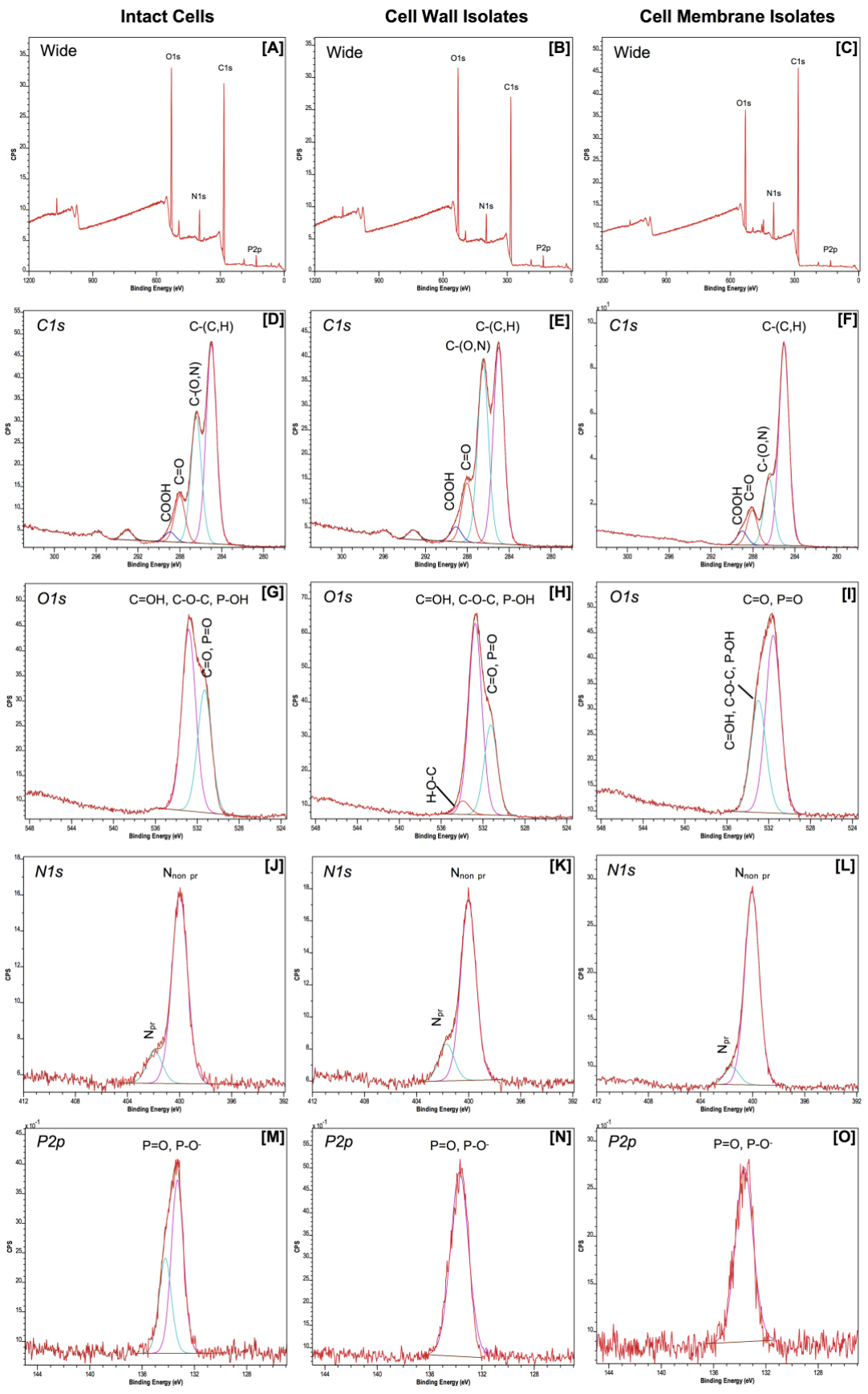

Supplementary Figure 2: XPS wide and high resolution C1s, O1s, N1s and P2p scans of intact *B. subtilis* 168 cells [A, D, G, J, M], cell wall isolates [B, E, H, K, N] and cell membrane isolates [C, F, I, L, O], respectively.

Supplementary Table 1: Speciation of U(VI) in solution in the presence of 0.1 M NaCl varied as a function of pH.

		% total concentration																				
Component	Species	0.125 mM			0.25 mM			0.5 mM			1 mM			2 mM			3 mM			4 mM		
		pH 3	pH 4.25	pH 5.5	pH 3	pH 4.25	pH 5.5	pH 3	pH 4.25	pH 5.5	pH 3	pH 4.25	pH 5.5	pH 3	pH 4.25	pH 5.5	pH 3	pH 4.25	pH 5.5	pH 3	pH 4.25	pH 5.5
UO_2^{2+}	UO_2^{2+}	93.44	84.88	6.67	93.36	80.63	4.26	93.20	80.63	2.69	92.88	64.28	1.69	92.26	52.81	1.05	92.71	44.63	0.80	92.10	39.81	0.66
	UO_2Cl^+	6.21	5.65	0.44	6.20	5.36	0.28	6.18	5.36	0.18	6.15	4.26	0.11	6.08	3.49	0.07	4.86	2.36	0.05	4.79	2.09	0.04
	$UO_2NO_3^+$	0.02	0.01		0.03	0.03		0.06	0.03		0.12	0.09		0.25	0.14		0.40	0.19		0.52	0.23	
	UO_2OH^+	0.24	3.81	5.32	0.24	3.61	3.39	0.23	3.61	2.14	0.23	2.87	1.34	0.23	2.35	0.84	0.24	2.10	0.63	0.24	1.86	0.52
	$(UO_2)_2(OH)_2^{2+}$	0.02	4.68	9.13	0.04	8.43	7.44	0.07	8.43	5.93	0.14	21.35	4.66	0.28	28.66	3.62	0.45	33.06	3.11	0.59	34.87	2.79
	$(UO_2)_3(OH)_5^+$		0.08	65.09		0.26	67.65		0.26	68.13		2.07	67.00		4.52	64.68		7.52	62.90		9.34	61.48
	$(UO_2)_4(OH)_7^+$			11.06			14.67			18.66		0.09	22.99		0.31	27.63		0.69	30.46		1.02	32.52
	$(UO_2)_3(OH)_4^{2+}$		0.04	2.05		0.15	2.13		0.15	2.15		1.16	2.11		2.55	2.05		4.02	1.99		5.01	1.95
	$(UO_2)_2OH^{3+}$	0.06	0.83	0.09	0.11	1.50	0.07	0.23	1.50	0.06	0.45	3.82	0.05	0.89	5.16	0.04	1.32	5.43	0.03	1.74	5.77	0.03
	$UO_2Cl_{2\ (aq)}$	0.03	0.02		0.03	0.02		0.03	0.02		0.02	0.02		0.02	0.01		0.02			0.02		
	$UO_2(OH)_{2\ (aq)}$			0.16			0.10			0.06			0.04			0.03			0.02			0.02
NO_3^-	NO_3^-	97.94	97.94	97.95	97.93	97.94	97.95	97.92	97.94	97.95	97.89	97.91	97.95	97.84	97.89	97.95	98.22	98.31	97.95	98.16	98.3	97.95
	$UO_2NO_3^+$				0.02	0.01		0.03	0.01		0.06	0.04		0.12	0.07		0.20	0.10		0.26	0.11	
	$NaNO_{3\ (aq)}$	2.05	2.05	2.05	2.05	2.05	2.05	2.05	2.05	2.05	2.05	2.05	2.05	2.04	2.04	2.05	1.59	1.59	2.05	1.58	1.59	2.05
Na^+	Na^+	96.41	96.40	96.40	96.40	96.40	96.40	96.40	96.40	96.39	96.39	96.39	96.38	96.37	96.36	96.36	97.12	97.11	96.33	97.10	97.09	96.30
	$NaCl_{(aq)}$	3.59	3.59	3.59	3.59	3.59	3.59	3.59	3.59	3.59	3.58	3.59	3.59	3.57	3.58	3.58	2.79	2.80	3.58	2.77	2.79	3.58
	$NaNO_{3\ (aq)}$							0.02		0.02	0.03	0.03	0.03	0.06	0.06	0.06	0.10	0.10	0.09	0.13	0.13	0.12
Cl^-	Cl^-	96.40	96.40	96.41	96.40	96.40	96.41	96.39	96.40	96.41	96.37	96.38	96.41	96.34	96.37	96.41	97.12	97.13	96.42	97.04	97.13	96.42
	UO_2Cl^+				0.01			0.02			0.05	0.03		0.09	0.05		2.79	0.07		0.19	0.08	
	$NaCl_{(aq)}$	3.59	3.59	3.59	3.59	3.59	3.59	3.59	3.59	3.59	3.58	3.59	3.59	3.57	3.58	3.59	0.10	2.80	3.58	2.77	2.79	3.58

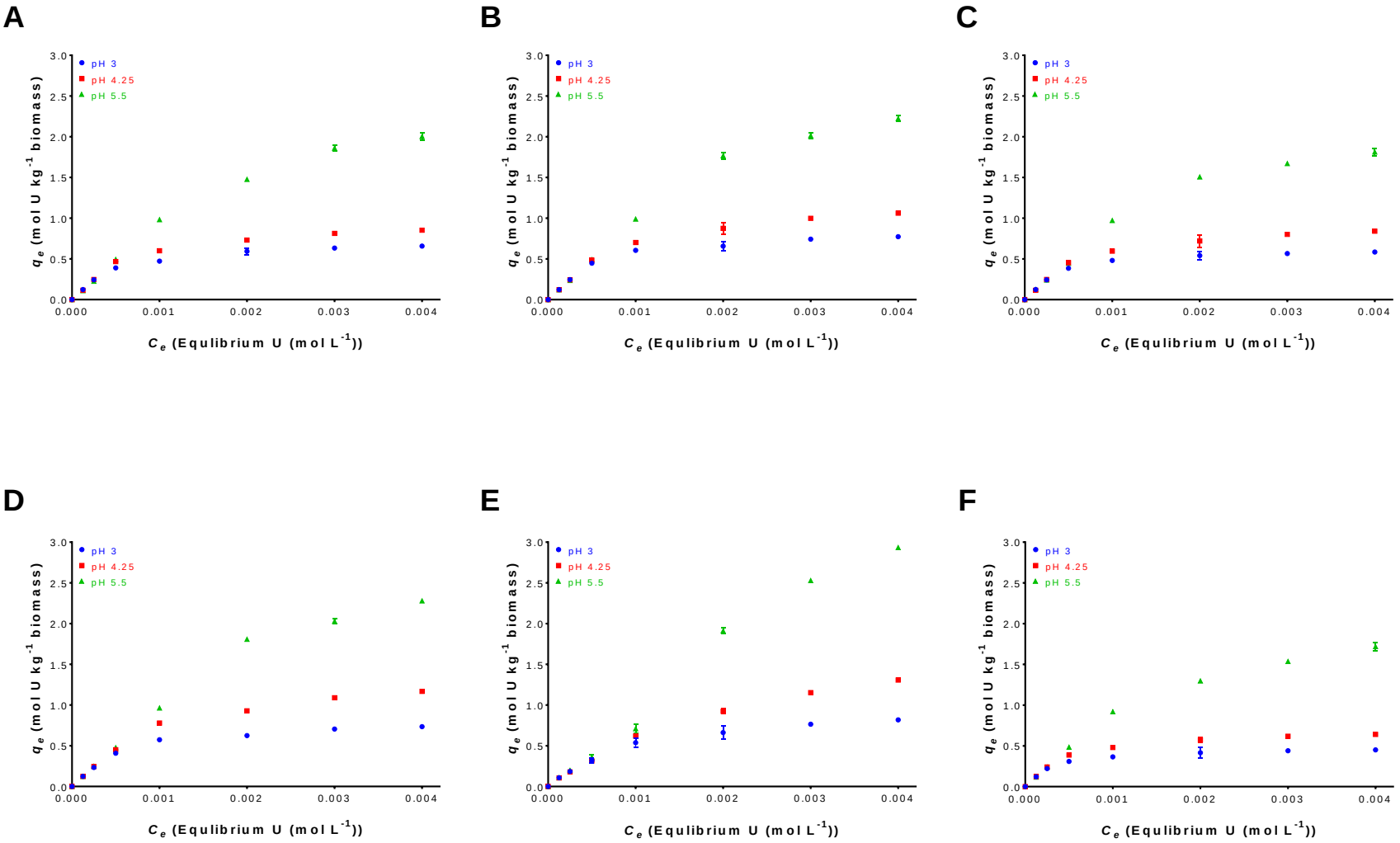

Supplementary Figure 3: Uranium biosorption isotherms for intact cells, cell wall and membrane isolates for *P. putida* 33015 [A-C] and *B. subtilis* 168 [D-F], respectively.

Supplementary Figure 4: Uranium biosorption isotherms for *P. putida* 33015 [A] and *B.subtilis* 168 [B], respectively. The solid line represents the fitting of the Freundlich adsorption model as calculated using the Freundlich constants and equation; $q_e = K_F \times {C_e}^{n_i}$

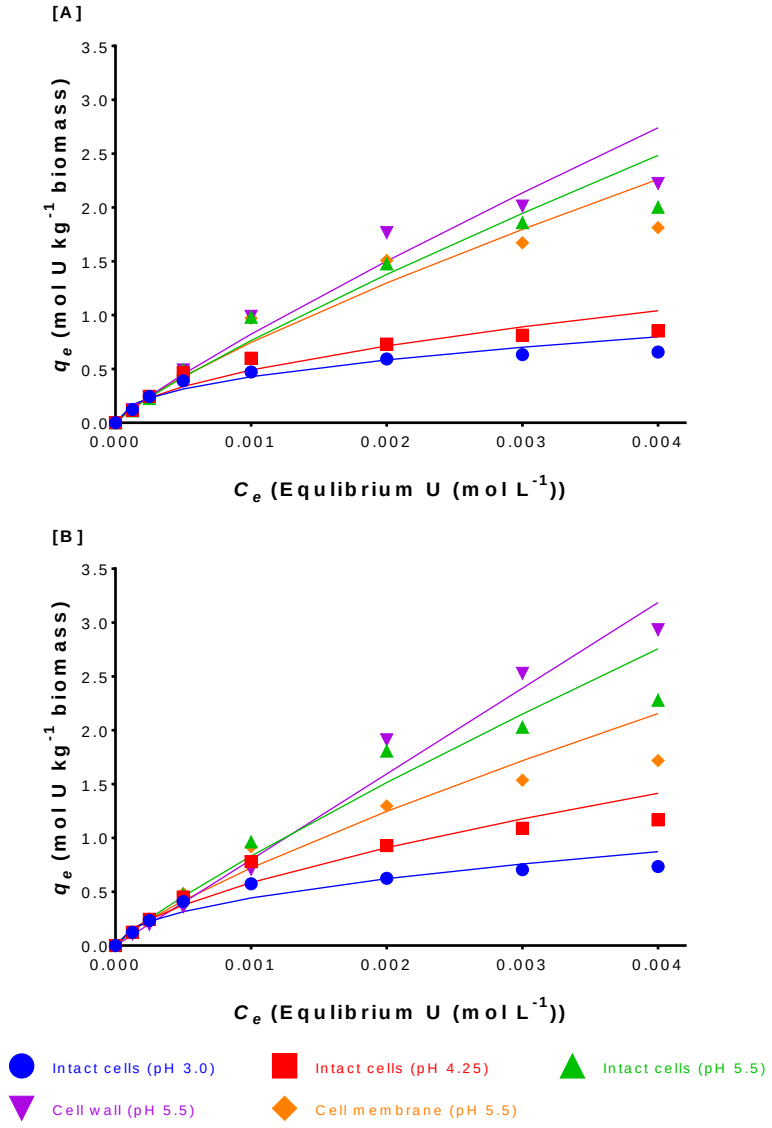

Supplementary Table 2: Constants obtained from Langmuir isotherms, at 298.15 K. The Langmuir isotherm was calculated by plotting the inverse of C_e vs. q_e. The corresponding linear regression was applied to the Langmuir equation ($\frac{1}{q_e} = \frac{1}{K_L \times Q_{max}} \times \frac{1}{C_e} + \frac{1}{Q_{max}}$), where the gradient (m) is $\frac{1}{K_L \times Q_{max}}$ and intercept (b) is $\frac{1}{Q_{max}}$. Q_{max} ($\frac{1}{b}$), K_L ($\frac{1}{m \times Q_{max}}$) and K_D ($K_L \times Q_{max}$) were calculated. Q_{max} was the maximum adsorption concentration of sorbate, K_L was the Langmuir constant and K_D the dissociation constant.

	pH	Q_{max} mol$_{-1}$ kg	K_L L$_{-1}$ mol	K_D K_L x Q_{max}	$\Delta G°$ kJ mol$_{-1}$
***Pseudomonas putida* 33015**					
Intact cells	3	0.934	1254.277	1171.783	-17.517
	4.25	1.967	510.700	1004.722	-17.136
	5.5	20.284	44.291	898.392	-16.858
Cell wall	3	1.397	789.677	1102.901	-17.367
	4.25	2.322	453.368	1052.632	-17.251
	5.5	10.741	91.266	980.296	-17.075
Cell membrane	3	0.875	1364.038	1193.175	-17.562
	4.25	1.875	53.684	100.644	-11.432
	5.5	4.686	21.678	101.585	-11.455
***Bacillus subtilis* 168**					
Intact cells	3	1.127	1001.806	1128.796	-17.424
	4.25	2.440	432.566	1055.298	-17.257
	5.5	9.050	111.414	1008.268	-17.144
Cell wall	3	1.020	929.648	948.137	-16.992
	4.25	1.403	635.853	892.299	-16.841
	5.5	6.588	130.435	859.254	-16.748
Cell membrane	3	0.553	231.157	127.747	-12.023
	4.25	0.919	127.324	117.069	-11.807
	5.5	5.339	181.951	971.440	-17.052

Supplementary Figure 5: Uranium biosorption isotherms for *P. putida* 33015 [A] and *B.subtilis* 168 [B], respectively. The solid line represents the fitting of the Langmuir adsorption model as calculated using the Langmuir constants and equation; $q_e = \frac{Q_{max} \times K_L \times C_e}{1 + K_L \times C_e}$.

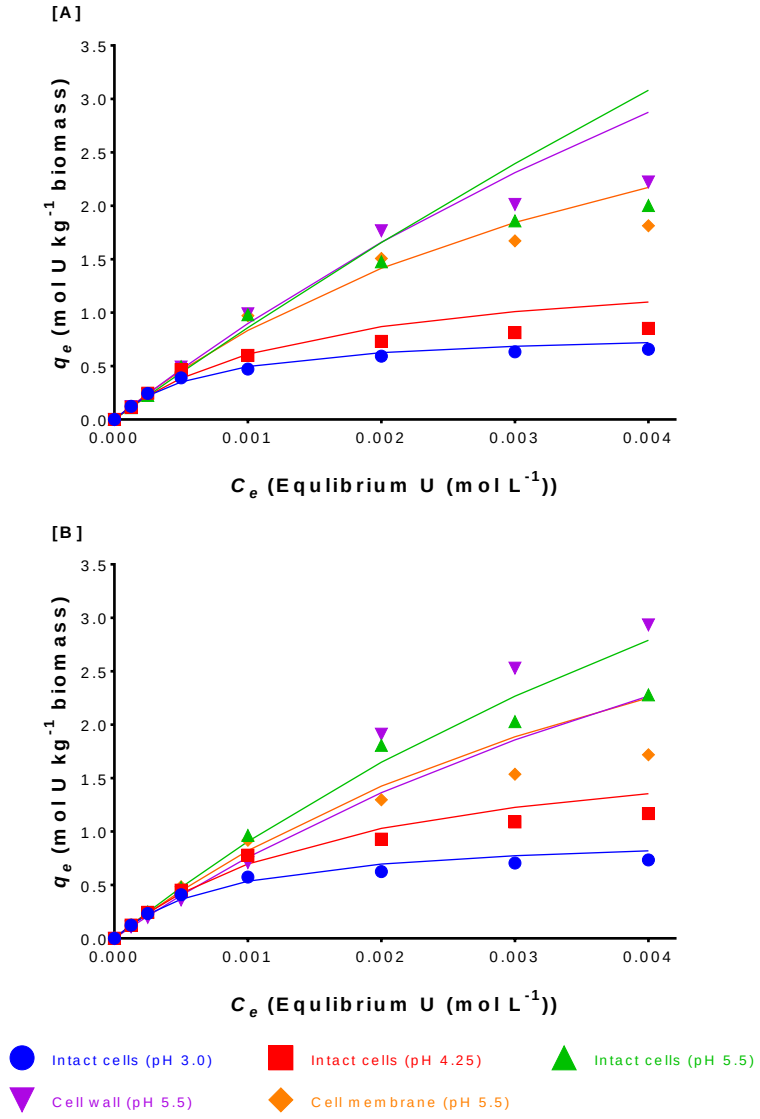

Supplementary Information 2: Detailed interpretation of FT-IR spectra of cell surface isolates

The cell wall isolates of *P. putida,* in comparison with intact cells, exhibited an increase in prevalence of adsorption bands characteristic of components of Gram-negative cell walls. Increases in the intensity of adsorption bands associated with fatty acids and lipids in the outer membrane of the Gram- negative cell wall were observed in the isolated components. Adsorption bands between 3000 – 2800 cm^{-1} were observed, corresponding to the vibrational stretching of CH_3 and CH_2, and a shoulder peak was observed at 1723 - 1734 cm^{-1}, that was not present in intact cell spectra, and attributed to the vibrational symmetric stretching of the carbon oxygen (C=O) bond from the increased relative abundance of lipids [8-12]. Changes in position, shape and increases in intensity of adsorption bands that correspond to phosphate and C-OH, C-O-C, C-C groups are associated with an increase in the relative concentration of cell wall polysaccharides, peptidoglycan, lipopolysaccharides (LPS) and the outer membrane phospholipids following purification of cell wall components [8, 13].

The increase in absorption intensity between 3000 - 2800 cm^{-1}, attributed to CH_3 and CH_2 vibrational stretching, indicated the presence of a lipid-rich isolate attributed to the phospholipids within the *P. putida* cell membrane [8, 9, 14]. Furthermore, an additional adsorption band at 1740 cm^{-1} was attributed to the vibrational stretching of the C=O lipid bond that was not observed in intact cells and greater than that observed in cell wall isolates since the membrane fraction contained a greater relative abundance of lipids than that of the Gram-negative cell wall. An increased in absorption band intensity at ~ 1232 cm^{-1} corresponding to phosphate asymmetric stretching confirmed a phospholipid-rich isolate in comparison to intact cells [8, 9].

ATR-FT-IR spectra confirmed the purification and concentration of cell-wall associated compounds of *B. subtilis* from intact cells. Substantial changes in the adsorption band associated with the vibrational stretching of C-OH, C-O and C-C of carbohydrates confirmed the increase in concentration of peptidoglycan and other cell wall associated polysaccharides. This band shifted from 1063 cm^{-1} in intact cells to 1052 cm^{-1} and significantly increased in intensity following purification of cell isolates. Adsorption spectra were normalised with respect to the amide I absorption band, the adsorption band characteristic of functional groups associated with bacterial proteins [15], and present in all isolates. Additionally, the shoulder at 1724 – 1740cm^{-1} in cell wall isolates was attributed to the vibrational stretching of C=O groups in (lipo)teichoic acids following fractionation and purification of cell wall compounds [15].

Similarly, *B. subtilis* cell membrane isolates were characteristed by an increased intensity of lipid-associated adsorption bands, 3000 – 2800 cm^{-1} and 1739 cm^{-1}, corresponding to greater relative abundance of phospholipid-rich biological molecules, compared to intact cells [8, 9, 14]. Small changes in the adsorption band position and intensity within the 1470 – 1350 cm^{-1} region suggested changes in protein and lipid content, from the presence of a greater abundance of membrane-associated proteins such as porins[16]. A decrease in intensity was observed for the carbohydrate associated ν (C-OH, C-0-C, C-C) absorption band at ~1065 cm^{-1} in the cell membrane isolates compared to intact *B. subtilis* cells. This was attributed to a lack of peptidoglycan and other polysaccharides that were once associated with the *B. subtilis* cell wall and removed during fractionation and purification [8, 9, 12]. Additionally, a decrease in intensity of the absorption band associated with phosphate vibrational asymmetric stretching (~ 1220 – 1230 cm^{-1}) was attributed to the source of phosphate associated only with the phospholipid bilayer, in comparison to additional phosphate associated with components of the cell wall and intracellularly of intact cells.

Supplement References

1. P. G. Rouxhet, N. Mozes, P. B. Dengis, Y. F. Dufrene, P. A. Gerin and M. J. Genet, *Colloids and Surfaces B-Biointerfaces*, 1994, **2**, 347-369.
2. Y. F. Dufrene, A. VanderWal, W. Norde and P. G. Rouxhet, *Journal of Bacteriology*, 1997, **179**, 1023-1028.
3. F. Ahimou, C. J. P. Boonaert, Y. Adriaensen, P. Jacques, P. Thonart, M. Paquot and P. G. Rouxhet, *Journal of Colloid and Interface Science*, 2007, **309**, 49-55.
4. J. J. Ojeda, M. E. Romero-Gonzalez, R. T. Bachmann, R. G. J. Edyvean and S. A. Banwart, *Langmuir*, 2008, **24**, 4032-4040.
5. M. Ramstedt, L. Leone, P. Persson and A. Shchukarev, *Langmuir*, 2014, **30**, 4367-4374.
6. S. T. Jackson and R. G. Nuzzo, *Applied Surface Science*, 1995, **90**, 195-203.
7. H. C. van der Mei, J. de Vries and H. J. Busscher, *Surface Science Reports*, 2000, **39**, 3-24.
8. M. J. Baker, J. Trevisan, P. Bassan, R. Bhargava, H. J. Butler, K. M. Dorling, P. R. Fielden, S. W. Fogarty, N. J. Fullwood, K. A. Heys, C. Hughes, P. Lasch, P. L. Martin-Hirsch, B. Obinaju, G. D. Sockalingum, J. Sule-Suso, R. J. Strong, M. J. Walsh, B. R. Wood, P. Gardner and F. L. Martin, *Nature Protocols*, 2014, **9**, 1771-1791.
9. L. Shakirova, M. Grube, R. Goodacre, M. Gavare, L. Auzina and P. Zikmanis, *Vibrational Spectroscopy*, 2013, **64**, 51-57.
10. M. L. Merroun, G. Geipel, R. Nicolai, K. H. Heise and S. Selenska-Pobell, *Biometals*, 2003, **16**, 331-339.
11. S. K. Kazy, P. Sar and S. F. D'Souza, *Bioremediation Journal*, 2008, **12**, 47-57.
12. J. J. Ojeda, M. E. Romero-Gonzalez and S. A. Banwart, *Analytical Chemistry*, 2009, **81**, 6467-6473.
13. S. J. Parikh and J. Chorover, *Langmuir*, 2006, **22**, 8492-8500.
14. A. A. Kamnev, L. P. Antonyuk, L. Y. Matora, O. B. Serebrennikova, M. V. Sumaroka, M. Colina, M. F. Renou-Gonnord and V. V. Ignatov, *Journal of Molecular Structure*, 1999, **481**, 387-393.
15. W. Jiang, A. Saxena, B. Song, B. B. Ward, T. J. Beveridge and S. C. B. Myneni, *Langmuir*, 2004, **20**, 11433-11442.
16. J. Wang and C. Chen, *Biotechnology Advances*, 2009, **27**, 195-226.